

Imaging Angiogenesis: Applications and Potential for Drug Development

Janet C. Miller, Homer H. Pien, Dushyant Sahani, A. Gregory Sorensen, James H. Thrall

Recognition of the importance of angiogenesis to tumor growth and metastasis has led to efforts to develop new drugs that are targeted to angiogenic vasculature. Clinical trials of these agents are challenging, both because there is no agreed upon method of establishing the correct dosage for drugs whose mechanism of action is not primarily cytotoxic and because of the long time it takes to determine whether such drugs have a clinical effect. Therefore, there is a need for rapid and effective biomarkers to establish drug dosage and monitor clinical response. This review addresses the potential of imaging as a way to accurately and reliably assess changes in angiogenic vasculature in response to therapy. We describe the advantages and disadvantages of several imaging modalities, including positron emission tomography, x-ray computed tomography, magnetic resonance imaging, ultrasound, and optical imaging, for imaging angiogenic vasculature. We also discuss the analytic methods used to derive blood flow, blood volume, empirical semiquantitative hemodynamic parameters, and quantitative hemodynamic parameters from pharmacokinetic modeling. We examine the validity of these methods, citing studies that test correlations between data derived from imaging and data derived from other established methods, their reproducibility, and correlations between imaging-derived hemodynamic parameters and other pathologic indicators, such as microvessel density, pathology score, and disease outcome. Finally, we discuss which imaging methods are most likely to have the sensitivity and reliability required for monitoring responses to cancer therapy and describe ways in which imaging has been used in clinical trials to date. [J Natl Cancer Inst 2005;97:172–87]

The realization that angiogenesis is an essential step for tumor growth and for the initiation of metastasis (1) has led to enormous interest in the discovery of angiogenic factors (2,3) and the development of drugs that target these molecules. However, many potential antiangiogenic therapies have not lived up to the expectations of preclinical trials (4), in part because of the difficulties in designing clinical trials for antiangiogenic drugs, which, unlike traditional chemotherapeutic agents, are not cytotoxic. Although this lack of cytotoxicity may be beneficial to the patient, it poses challenges for selecting the most effective dose and, therefore, determining clinical response.

The standard paradigm for selecting the dose of chemotherapeutic agents, the maximum tolerated dose, is not appropriate for antiangiogenic drugs (5) because the side effects of such drugs are not predictable and because the most effective dose may be much less than the maximum tolerated dose. On the other hand,

establishing the optimal dose of an antiangiogenic agent by measuring tumor shrinkage or time to disease progression is impractical because each may take months or years to assess. Furthermore, it has been speculated that tumor shrinkage may be slower with antiangiogenic therapy than with traditional chemotherapy (6). In addition, cancers are heterogeneous and variations in individual response to cancer therapy vary widely. Thus, to obtain statistically significant results, large populations would be needed in long, and therefore expensive, clinical trials. There is, therefore, a great need to establish reliable biomarkers of early responses to noncytotoxic drugs, which predict subsequent clinical response. Such biomarkers would not only facilitate clinical trials of new drugs but could also be used to aid in the selection of optimal treatment for individual patients (5,7–10).

Although clinical responses to cancer therapy are slow, some metabolic and physiologic responses occur soon after the start of therapy. Some of these latter responses may be associated with drug toxicity or side effects, but others may foreshadow a clinical response. Because antiangiogenic and antineovascular therapies are designed to affect the abnormal blood vessels found in tumors, changes in blood volume, blood flow, or other hemodynamic parameters may be promising biomarkers that herald a positive clinical response to therapy.

Angiogenic vasculature in tumors differs from that in healthy tissue in several respects. Chronic overproduction of proangiogenic factors in tumors leads to uncontrolled development of new blood vessels. As a result, the number of blood vessels within a given microscopic area (i.e., microvessel density) is usually high but rarely uniform. Tumor blood vessels are typically dilated and tortuous, with abnormal branching patterns, dead ends, and no organization into arterioles, capillaries, and venules (Fig. 1). Blood flow within tumors is spatially and temporally heterogeneous and, sometimes, even oscillating. In addition, because angiogenic factors increase vascular permeability, blood vessels of tumors may be an order of magnitude more permeable than those of normal tissue (11–13).

Microvessel density is a prognostic indicator for many cancers. Therefore, the assessment of microvessel density in biopsy samples taken over the course of treatment would seem to be a

Affiliation of authors: Center for Biomarkers in Imaging, Department of Radiology, Massachusetts General Hospital, Boston, MA.

Correspondence to: Janet Cochrane Miller, DPhil, Department of Radiology, Massachusetts General Hospital, 100 Charles River Plaza, Boston, MA 02114 (e-mail: jcmiller@partners.org).

See “Notes” following “References.”

DOI: 10.1093/jnci/dji023

Journal of the National Cancer Institute, Vol. 97, No. 3, © Oxford University Press 2005, all rights reserved.

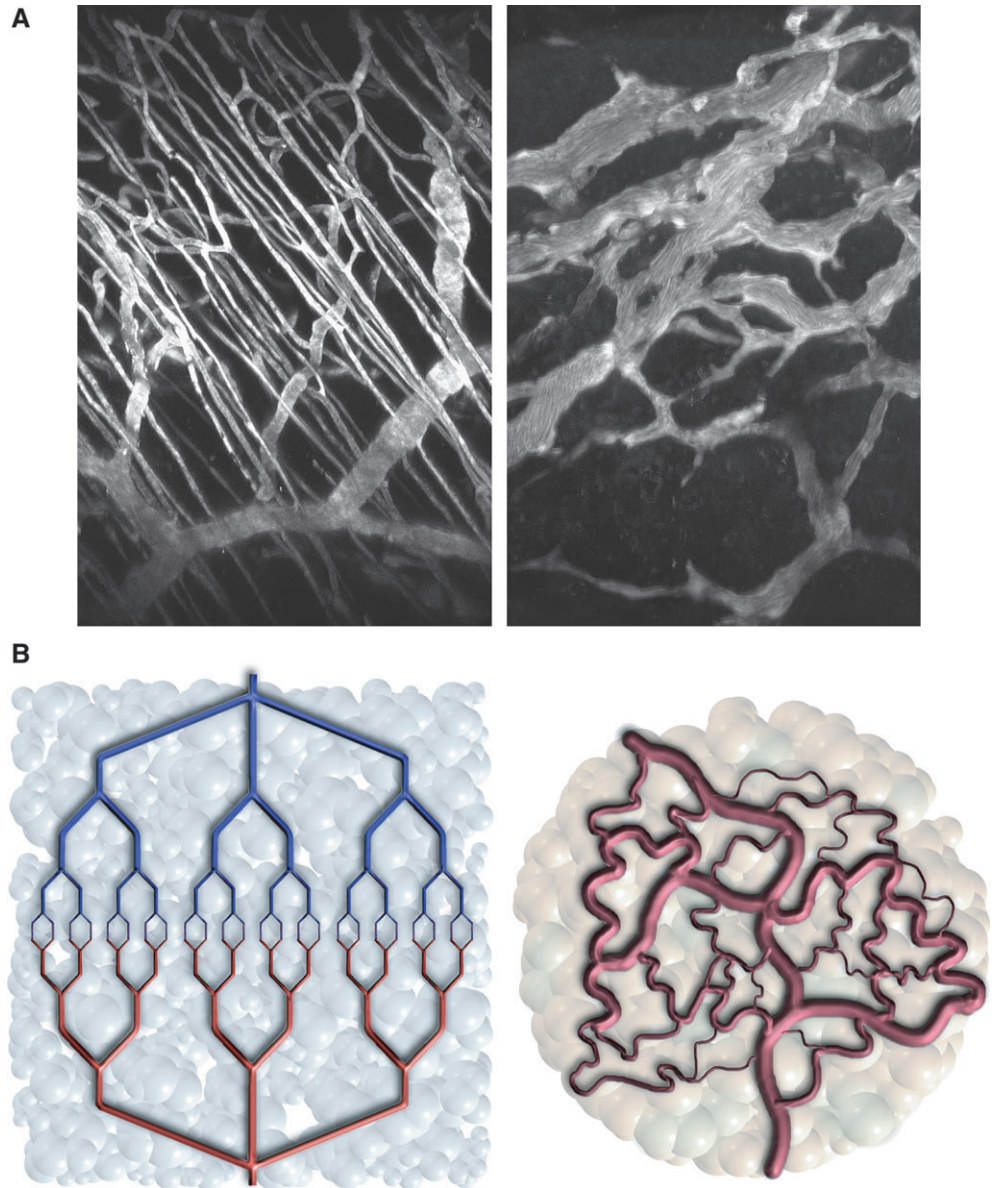


Fig. 1. Microvascular structure. Well-organized normal vasculature, as shown in a photomicrograph of rodent vasculature in the **left panel** of **A** and in a schematic representation in the **left panel** of **B**. Chaotic abnormal angiogenic vascular network in tumor, as shown in a photomicrograph of rodent tumor vasculature in the **right panel** of **A** and in a schematic representation in the **right panel** of **B**. In **B**, red corresponds to oxygenated arterial blood, blue corresponds to oxygen-depleted venous blood, and purple corresponds to poorly oxygenated blood. From Jain et al. (11), with permission.

straightforward strategy to monitor the efficacy of antiangiogenic therapy. However, this approach is not only invasive but also probably unreliable because the greatest density of new vessels (i.e., angiogenic “hot spots”) is typically found in the tumor periphery and, as the tumor grows, the central portion of the tumor may become hypovascular and even necrotic. Therefore, it is difficult to obtain comparable biopsy samples to accurately quantify tissue response (14). In addition, effective antiangiogenic therapy will not only affect capillaries but also result in tumor cell elimination. Therefore, the degree to which the effects on capillaries and tumor cells are coupled will affect microvessel density (6).

Imaging of angiogenic vasculature may be a better alternative than measuring microvessel density for assessing therapy because it is noninvasive and can be used to assess much larger volumes than biopsy samples (3,5,8–10). Several imaging methods have been developed to measure blood volume and blood flow, as well as differences in blood vessel permeability, vascular size, and oxygenation. However, there is no general agreement as to which imaging methods are most suitable for

monitoring antiangiogenic therapy in single-center and multi-center trials.

In this review, we examine the validity and reproducibility of different imaging methods that have been used to determine vascular and hemodynamic parameters. We discuss the strengths and weaknesses of various imaging techniques, as well as the robustness of the vascular and hemodynamic parameters derived from each technique. Finally, we illustrate how various methods for imaging angiogenesis have been used in clinical trials of cancer therapy and discuss preliminary data suggesting that early changes in the angiogenic vasculature in response to antiangiogenic therapy correlate with clinical response.

IMAGING MODALITIES FOR DETECTING ANGIOGENESIS

Modalities used to image angiogenic vasculature include x-ray computed tomography (CT), magnetic resonance imaging (MRI), positron emission tomography (PET), single-photon emission computed tomography (SPECT), ultrasound,

Table 1. Advantages and disadvantages of some modalities used for steady-state and dynamic contrast imaging of microvasculature*

Modality	Contrast agents	Sensitivity†	Voxel size	Advantages	Disadvantages
MRI	Gd-DTPA USPIO	+++	1.5 mm (dynamic) 0.4–0.8 mm (steady state)	Low toxicity of contrast agents Imaging of intrinsic nuclei possible No ionizing radiation Versatility in pulse sequences	Susceptible to motion Instrument variation Limited number of scan slices Imaging indirect effects of paramagnetism
	Hb Hydrogen (intrinsic contrast)	+		Variety of available contrast agents and several more in development Sensitive to vessel size	Dynamic imaging limited to 5–20 slices
MD CT	Iodinated agents	+	0.5–0.8 mm	Absorption directly proportional to concentration of contrast agent	Low sensitivity to contrast Contrast agent toxicity Exposure to ionizing radiation Dynamic imaging limited to 5–20 slices
PET	¹⁵ H-H ₂ O	+++++	3–4 mm	Emission directly proportional to concentration of contrast agent	Very short radionuclide half-life
	¹¹ C-CO C ¹⁵ O			Whole body imaging	Limited availability
SPECT	^{99m} Tc-RBC	++++	5–6 mm	Emission directly proportional to concentration of contrast agent Whole body imaging	
Ultrasound	None	++	0.5 mm	Inexpensive, widely available	Doppler imaging not sensitive to blood vessels smaller than 100 μm in diameter
	Microbubble	++++		Microbubbles confined within blood pool Highly sensitive detection of microbubbles	Limited depth penetration Operator dependent
Near infrared optical	Hb, HbO ₂ Indocyanine green	+	1–2 cm	Inexpensive Portable	Limited depth penetration No standard instrumentation

*MRI = magnetic resonance imaging; MD CT = multi-detector x-ray computed tomography; PET = positron emission tomography; SPECT = single-photon emission computed tomography; Gd-DTPA = gadolinium diethyltriamine pentaacetic acid; USPIO = dextran-coated ultra-small particles of iron oxide; Hb = deoxy-hemoglobin; HbO₂ = oxyhemoglobin; ^{99m}Tc-RBC = ^{99m}Tc-labeled red blood cells; ^{99m}Tc-DTPA-HSA = ^{99m}Tc- diethylamine pentaacetic acid-labeled human serum albumin.

†Sensitivity is a relative measure of the amount of contrast agent detected or image enhancement, from highest (+++++) to lowest (+).

and near-infrared optical imaging. Methods have been developed to measure blood volume, blood flow, and several semiquantitative and quantitative kinetic hemodynamic parameters (9,13–17). Data on the relative size of blood vessels can be gleaned from MRI (18), and both MRI (19–21) and near-infrared optical imaging (22) are sensitive to tissue oxygenation. Characteristic markers of angiogenesis, such as vascular endothelial growth factors (VEGFs) or α_vβ₃ integrin, can be visualized with the aid of molecular imaging agents, which are hybrid molecules that combine one component that can be detected by imaging and another that binds to or interacts with a target molecule (7,23,24). No single imaging modality is ideal in all circumstances; each has strengths and weaknesses with respect to its availability, sensitivity, ease of accurate and reproducible quantification, the regions of the body that can be imaged, the availability of compatible intravascular contrast agents, and contrast agent toxicity (Table 1).

Several different MRI methods have been devised for angiogenic imaging, using both extrinsic and intrinsic contrast agents (Table 1). MRI is a practical modality for assessing vascular changes over time because it is already widely used clinically to assess tumor growth. The commonly used contrast agent, gadolinium diethyltriamine pentaacetic acid (Gd-DTPA), has low toxicity and because MRI does not involve ionizing radiation, repeat imaging is therefore limited mainly by instrument availability and expense. In MRI, high-field magnets align paramagnetic nuclei, such as hydrogen, and radiofrequency pulses are used to perturb the orientation and nuclear spin of the nuclei. Magnetic resonance

images are derived from the rate of energy release due to realignment of hydrogen nuclei to the magnetic field (T1 recovery) and spin–spin relaxation or loss of transverse magnetism (T2 decay), which depends largely on the chemical bonding of the hydrogen nuclei. MRI contrast agents contain paramagnetic nuclei, such as gadolinium, which increase the rates of T1 recovery and T2 decay, thereby altering the measured signals. At high concentrations the primary effect of Gd-DTPA is to diminish T2 signals, whereas at low concentrations, the primary effect is to enhance T1 signals.

MRI estimates of angiogenic blood volume and flow are generally calculated relative to that of normal tissue because the changes in signal strength are not linear over the range of concentrations of gadolinium found and because Gd-DTPA passes through the vasculature and permeates tissues. Because the concentration of Gd-DTPA is initially high, first-pass T2-weighted imaging is, in general, sensitive to blood flow and blood volume. T1-weighted imaging is very sensitive to the low concentrations of Gd-DTPA that permeate through capillary walls in angiogenic vasculature, which may make MRI more reliable than other imaging modalities for measuring parameters that are dependent on permeability. Intravascular MRI contrast agents, which are more accurate for measuring blood volume, may become available in the future. Several of these agents have been developed (25–28), and some have been used extensively in clinical trials (29,30). The disadvantage with MRI, however, is that MRI protocols and instrument performance have substantial effects on signal

strength, making it difficult to compare data obtained with different instruments.

Hemodynamic data from CT imaging may be more quantitative than data obtained by MRI because the change in CT image intensity due to the contrast agent is linearly related to the concentration of the contrast agent. In addition, CT has the highest spatial resolution of all imaging modalities. However, the sensitivity of CT is limited, and high concentrations of CT contrast agent are required, which can cause toxic effects. This toxicity, together with the relatively high doses of radiation needed, limits the use of CT for repeated scanning.

Both PET and SPECT imaging are highly quantitative and sensitive to very low concentrations of tracer molecules. PET, which is able to detect picomolar concentrations of tracer, is approximately 10 times more sensitive than SPECT (31). Both methods are well suited to molecular imaging because of the generally low concentrations of target molecules, as well as for gathering hemodynamic data. However, because the radionuclides used in PET tracers have a very short half-life (2 minutes for ^{15}O , 20 minutes for ^{11}C , and 10 minutes for ^{13}N), PET can only be performed at facilities that have a PET scanner and the necessary cyclotron and chemical laboratory for the preparation of the tracers. The radionuclides used for SPECT are easier to prepare and somewhat longer lived than those used for PET (6 hours for $^{99\text{m}}\text{Tc}$, 67 hours for ^{111}In , and 13.2 hours for ^{123}I), and SPECT imaging is much more widely available than PET imaging. However, both PET and SPECT images are of lower spatial resolution than magnetic resonance (MR) or CT images.

Although ultrasound imaging is inexpensive, portable, and widely available, its value depends on the skill of the operator, and it produces images that have low spatial resolution compared with those produced by MRI or CT. However, very low concentrations of micron-sized gas-filled microbubble contrast agents can be detected by ultrasound, and these are useful agents for angiogenic imaging. Microbubbles are true intravascular contrast agents and are useful for measuring blood volume and flow (32), although the calculated values obtained by using these agents are not absolute but relative to those in other tissues at similar depths. In addition, microbubbles labeled with agents that bind to angiogenic markers, such as $\alpha_v\beta_3$ integrin, are useful for molecular imaging of angiogenic vasculature (98).

Optical technologies, such as near-infrared spectroscopic diffuse optical tomography (33,34) and orthogonal polarization spectroscopy (35), are being developed as alternative modalities for imaging characteristics of angiogenic vasculature. Near-infrared light penetrates tissue sufficiently well to allow one to obtain low-resolution images of tissues to a depth of a few centimeters, and the regional concentration of hemoglobin and oxygen saturation can be calculated from the absorption of hemoglobin and deoxyhemoglobin. Orthogonal polarization spectroscopy has been used to monitor antivascular therapy of superficial tumors (36). Indocyanine green, a clinically available contrast agent that fluoresces at near-infrared wavelengths, has been used to image angiogenic vasculature in breast tumors (37,38). In addition, sensitive molecular imaging agents have been developed that fluoresce when they are acted upon by enzymes that are associated with angiogenesis, such as matrix metalloproteases (39). Optical imaging has the advantage of being relatively inexpensive and portable, but it is still under development and is not yet widely available.

HEMODYNAMIC PARAMETERS THAT CAN BE DERIVED FROM IMAGING DATA

Blood Volume

Measuring changes in blood volume as a way to monitor the efficacy of therapy is of potential value because tumors have high microvessel density as well as larger blood vessels than normal tissue. Blood volume can be calculated from the difference in image intensity in the absence and presence of a contrast agent. Steady-state imaging methods are suitable when intravascular contrast agents are used, whereas dynamic imaging methods are suitable for contrast agents that permeate the vascular endothelium.

Steady-state imaging. Blood volume is directionally proportional to the regional concentration of contrast agent or tracer, provided that the agent remains confined within the vasculature at a constant concentration throughout the imaging period. PET imaging of ^{15}O - or ^{11}C -carboxyhemoglobin, which is formed after subjects have inhaled trace quantities of radiolabeled carbon monoxide, is a highly sensitive, accurate, and reproducible steady-state method for measuring blood volume (40,41) (Table 2), as is SPECT imaging of red blood cells that are labeled with $^{99\text{m}}\text{Tc}$ and injected into the subject (42,43). SPECT imaging of $^{99\text{m}}\text{Tc}$ -labeled human serum albumin has also been validated in normal vasculature (43) but may leak out of angiogenic vasculature. Ultrasound imaging using microbubble contrast agents is an alternative method (32) that has been used to estimate blood volume, and the results have been shown to correlate with estimates derived from MRI data (44).

There are no CT or MRI contrast agents that are confined reliably within tumor vasculature. Ultra-small iron oxide particles (USPIO), which are intravascular in normal vasculature (29,30), have been shown to extravasate from tumor vasculature (45) and do not provide accurate estimates of blood volume in tumors from steady-state imaging methods (Table 2) (47).

Dynamic contrast imaging. In this method, a bolus of contrast agent is injected into a vein, and rapid imaging techniques are then used to acquire serial images of a limited number of slices as the agent enters and leaves the tissue. For most clinical multidetector CT instruments, data collection is limited to a 2-cm "slab," whereas MRI can acquire data from about 11 slices by sacrificing image resolution for a greater volume of tissue scanned. The concentration of contrast agent in each voxel of the serial images can be depicted as a broad peak (the enhancement curve), which corresponds to the arrival and departure of the agent. Arrival time in each voxel is affected by the individual's cardiac output at the time of imaging as well as by variations in blood flow between small and large blood vessels, which also cause some dispersal of the agent.

Blood volume in the tissue is proportional to the area under the enhancement curve (AUC), provided that the agent remains within the vasculature during the scan. CT dynamic contrast imaging estimates of blood volume are fully quantitative, although MR dynamic contrast imaging data are not, especially at low concentrations of Gd-DTPA, which occur as Gd-DTPA leaves the tissue (the tail end of the enhancement curve). Therefore, different methods of selecting the cut-off point of the AUC have been developed to obtain consistent estimates of blood volume (56). In addition, MRI estimates of blood volume are expressed as a ratio to that in another tissue or to normal tissue of the same type, whereas CT estimates are absolute. Nevertheless,

Table 2. Validity and reproducibility of estimates of blood volume or fractional plasma volume*

Imaging method (contrast agent)	Validation method (model system)	Correlation coefficient or ratio (reference)	Reproducibility study (model system)	Variation (reference)
PET (^{11}CO or C^{15}O)	^{51}Cr -labeled radiotracer Blood concentration of ^{15}O	Ratio 1.02 ± 0.03 (40) $r = .73, P < .001$ (46)	Two consecutive studies (human muscle)	Mean CoV = $3.0 \pm 1.8\%$ (46)
SPECT ($^{99\text{m}}\text{Tc}$ -RBC)	Blood concentration of $^{99\text{m}}\text{Tc}$	$r = 1.0$ (43)	Two serial studies (human brain)	$P < .001$ (42)
SPECT ($^{99\text{m}}\text{Tc}$ -DTPA-HSA)			No data found	
US (microbubble)	Gd-DTPA MRI amplitude, fPV (human tumor xenograft)	$r = .61, P = .001$ (44)		
MRI (USPIO†)	Fractional volume from latex perfusion and histology (normal brain) (glioma)	$r = .83\ddagger, P = .03$ $r = .37\ddagger, P = .27$ (47)	Study repeat after 4 weeks (normal brain)	Mean ratio = 1.08 CoV = 12%, $r = .84, P < .0001$ (48)
	$^{99\text{m}}\text{Tc}$ radiotracer (mice, experimental tumors)	Ratio 1.05 ± 0.03 (49)	No data found	
MRI (MPEG-PL-Gd-DTPA)	Phantom studies, agreement with literature (normal brain and glioma, rats)	$R^2 = .999$, up to $2 \mu\text{M Gd}$ (50)	No data found	
MRI (albumin-Gd-DTPA)	MRI (USPIO) Radiotracer (breast tumor xenograft):	$r = .60, P < .1$ (51) $R^2 = .99$ (15)	No data found	
MD CT (iodinated contrast)	Phantom	$R^2 = .996, P < .001$ (52)	Two consecutive studies (rabbit brain tumor)	Variability = 7.3% (53)
MRI (Gd-DTPA)	C^{15}O PET (pig brain)	$R^2 = .67$, slope 0.45 ± 0.11 (54)	Study repeated after 2 days (human gliomas)	$r_1 = .981$ (55)

*The correlation of blood volume or fractional plasma volume measured from imaging data with that measured by another method or the ratio and standard deviation of the two methods. MRI = magnetic resonance imaging; MD CT = multidetector x-ray computed tomography; PET = positron emission tomography; SPECT = single-photon emission computed tomography; $^{99\text{m}}\text{Tc}$ -RBC = $^{99\text{m}}\text{Tc}$ -labeled red blood cells; $^{99\text{m}}\text{Tc}$ -DTPA-HSA = $^{99\text{m}}\text{Tc}$ -diethylenetriamine pentaacetic acid-human serum albumin; US = ultrasound; Gd-DTPA = gadolinium diethylenetriamine pentaacetic acid; fPV = fractional plasma volume; USPIO = dextran-coated ultra-small particles of iron oxide; MPEG-PL-Gd-DTPA = methoxy polyethylene glycol-poly-L-lysine-gadopentetate diglutamine (an experimental intravascular contrast agent); albumin-DTPA = albumin-diethylenetriamine pentaacetic acid (an experimental intravascular contrast agent); r = Pearson correlation coefficient; R^2 = correlation coefficient and slope from multiple regression analysis; mean CoV = mean coefficient of variation of repeated measurements \pm standard deviation; r_1 = intraclass correlation coefficient of the repeated measurements.

†Several similar products are under development: Ferumoxtran Sinerem (Guerbet, Aulney-sous-bois, France); Combidex (Advanced Magnetics, Cambridge, MA); Feruglose Clariscan (Amersham Health, Amersham, England), Ferumoxtran and Combidex are in phase III clinical trials.

‡Spearman's correlation coefficient.

estimates of blood volume from dynamic contrast MRI have been shown to be reproducible in patients with gliomas, despite some leakage of contrast agent into the tumor (Table 2). However, substantial leakage of contrast agents will result in invalid estimates, in which case blood volume must be derived from pharmacokinetic modeling (see below).

Several methods can be used to improve the accuracy of dynamic contrast imaging, such as the use of a power injector to obtain a consistent rate of administration of contrast agent. Power injectors are routinely used to inject the relatively large volumes of contrast agent needed for CT imaging but are not used in clinical applications of MR dynamic contrast imaging. Data accuracy can also be improved by correcting for contributions from large blood vessels (partial volume effect) through elimination of data from voxels with exceptionally high values (52,57,58).

Blood Flow

Measuring blood flow in tumors also has potential for assessing changes in angiogenic vasculature because the blood flow in tumors is usually abnormal. Two basic methods can be used to derive imaging data on blood flow: measuring the rate of tissue accumulation of a freely diffusible tracer or dynamic contrast imaging.

The rate of tissue accumulation of a freely diffusible tracer is limited only by the rate of blood flow and, therefore, is propor-

tional to blood flow (59). This principle has been applied to measure blood flow using PET with H_2^{15}O as a tracer and MRI arterial spin labeling. In PET, serial imaging of H_2^{15}O accumulation is used to measure the rate of accumulation of ^{15}O in tissue. Direct arterial blood sampling allows the concentration of tracer in the tissue to be expressed in terms of the arterial tracer concentration, the diffusion rate constant, and the blood flow. This technique is independent of instrument calibration and is regarded to be the most accurate method for measuring regional blood flow (Table 3) (60,61).

In arterial spin labeling MRI, water molecules are labeled by inverting the nuclear spin of their hydrogen atoms by a magnetic or radiofrequency pulse directed at arterial blood upstream of the region of interest (62–64). The change in the magnetic resonance signal as the labeled water in the arterial bloodstream arrives in the region of interest is used to determine an absolute value for blood flow. However, the sensitivity and spatial resolution of this method are limited, especially if the rate of blood flow is low, because the spin label is very short-lived. The signal-to-noise ratio of arterial spin labeling MRI is relatively low, but it can be improved by increasing the scan time (although increasing the scan time makes the technique more sensitive to patient movement). Nevertheless, arterial spin labeling is a reproducible method for measuring blood flow (Table 3) that does not require the use of any exogenous contrast agent, which makes it suitable for repeated measurements.

Table 3. Validity and reproducibility of measurements of blood flow*

Imaging method (contrast agent)	Validation method (model system)	Correlation coefficient (reference)	Reproducibility study (model system)	Variation (ref)
PET (H_2^{15}O)	Arterial injection of $^{15}\text{H}_2\text{O}$ bolus and blood sampling (baboon brain)	$R = .96, P = .001$ (60)	Two consecutive studies (human brain)	Mean difference \pm SD = $4.6 \pm 6.4\%$; $r = .9297$ (65)
			Study repeated within 2 days (human brain)	
			Gray matter	Mean difference \pm SD = $0.49 \pm 5.27 \text{ mL} \times \text{min}^{-1} \times 100 \text{ g}^{-1}$
			White matter	Mean difference \pm SD = $1.14 \pm 4.16 \text{ mL} \text{ min}^{-1} \times 100 \text{ g}^{-1}$ (66)
PET (C^{15}O_2)†	Radiolabeled microspheres (dog myocardium)	$R = .91$ (67)	Repeat studies after 30 min, 1 wk, and 2 wk (breast cancer)	Errors up to $\pm 10\%$ ‡ (68)
MRI arterial spin labeling	^{123}I -Indoamphetamine SPECT (human brain)	$R = .50, P < .0001$ (69)	Study repeated on separate 2 days (human brain)	
			Gray matter	Mean difference \pm SD = $-1.7 \pm 6.9 \text{ mL} \times \text{min}^{-1} \times 100 \text{ g}^{-1}$
	MRI, Gd-DTPA (glioma)	$R = .83, P < .05$ (70)	White matter	Mean difference = $-1.4 \pm 4.7 \text{ mL} \times \text{min}^{-1} \times 100 \text{ g}^{-1}$ (71)
MRI (Gd-DTPA)	$^{99\text{m}}\text{Tc}$ -HMPAO SPECT (human brain)	$R = .79, P < .001$ (72)	Study repeated within 2 days (human brain)	
			Gray matter	Mean difference \pm SD = $6.35 \pm 21.06 \text{ mL} \times \text{min}^{-1} \times 100 \text{ g}^{-1}$
			White matter	Mean difference \pm SD = $2.60 \pm 15.64 \text{ mL} \times \text{min}^{-1} \times 100 \text{ g}^{-1}$ (66)
Ultrasound (microbubble)	Radiolabeled microspheres (dog myocardium)	Mean $R = .96$, range = $.71-.99$ (73)	No data found	
MD CT (iodinated contrast)	Fluorescent microspheres (rabbit brain)	$R = .837, P = .001$ (52)	Two consecutive studies (rabbit brain)	Variability = 32.5% § (52)
	^{15}O - H_2O PET (normal human brain, glioma)	$R^2 = .64$ (74)	Two consecutive studies (Rabbit brain and brain tumors)	Variability = 13% § (53)
	$^{15}\text{H}_2\text{O}$ PET (human brain)	$R = .69$ (75)	Study repeated after 24 h (human glioma)	$r = .884$ (76) Variability = 13% (77)

*PET = positron emission tomography; MRI = magnetic resonance imaging; Gd-DTPA-HSA = Gd-diethyltriamine pentaacetic acid; $^{99\text{m}}\text{Tc}$ -HMPAO = $^{99\text{m}}\text{Tc}$ -hexamethylpropylene, a freely diffusible nuclear imaging agent; SPECT = single-photon emission computed tomography; MD CT = multidetector x-ray computed tomography; SD = standard deviation; $R =$; $r =$ Pearson correlation coefficient; $R^2 =$ correlation coefficient and slope from multiple regression analysis; $r_1 =$ intraclass correlation coefficient of the repeated measurements.

† ^{15}O is rapidly transferred to water after inhalation.

‡Estimated error for single observations.

§Variability determined from repeated studies using one-way analysis of variance.

||Statistical method not given.

Dynamic contrast imaging of blood flow. Dynamic contrast imaging can be used to accurately measure blood flow, provided that substantial amounts of tracer do not leak into the tissues. Within each voxel, the enhancement curve combines data for the arrival and departure of the contrast agent from blood vessels of all sizes. Because blood flow through the arteries and arterioles is faster than that in the microvasculature, an enhancement curve is obtained from an artery near the region of interest, and these data are used as an arterial input function to deconvolve arterial and tissue enhancement curves within the region of interest. Reproducible automated methods to determine the arterial input function from imaging data have recently been developed (78,79), although it is not yet clear whether their use improves accuracy. The mean blood flow (BF) can be calculated from the relationship (52,80): $\text{BF} = \text{BV}/\text{MTT}$, where BV is the blood volume

and MTT is the mean transit time, calculated from the enhancement curves.

Intermittent sonography using microbubble agents is a form of dynamic contrast imaging that is used to measure blood flow. While microbubbles are circulating in the bloodstream, a high-energy ultrasound pulse is applied to the region of interest, destroying the microbubbles there. The rate of increase in microbubble concentration is measured as they are replenished by blood flow. Calculations of blood flow derived from fitting the enhancement curve to an exponential model correlate well with absolute measures of blood flow in phantom studies and in ex vivo veins as well as with well-validated alternate methods, such as blood sampling of radiolabeled microspheres, in animal studies of blood flow in the myocardium (73) (Table 3) and renal cortex (81). A new mathematical model has been developed that

takes into account the substantial variability of blood flow in tumors (82). The two methods produced similar results for blood flow in healthy tissue, but in tumors, blood flow estimates were statistically significantly lower when measured by the latter method. Unfortunately, there is no gold standard to establish the validity of the newer method because phantom models do not model flow irregularities found in tumors (82).

Semiquantitative and Quantitative Hemodynamic Parameters

Several semiquantitative hemodynamic parameters have been derived from enhancement curves acquired from dynamic contrast imaging. These parameters include the initial and steepest slope of the curve, the time taken to reach 90% of the maximum enhancement (change in intensity), and the maximum enhancement attained after injection of a bolus of contrast agent (83,84). Prolonged changes in signals due to extravasation of contrast agent are seen in both MRI and CT imaging, especially in the more permeable angiogenic vasculature of tumors.

Semiquantitative parameters that are determined from MRI data are very dependent on instrument performance, making it difficult to compare data from different institutions that use different instrumentation and imaging protocols (85,86). Instrument variability is less of a problem with CT; Siemens (Erlangen, Germany) and Philips (Best, Netherlands) have software packages that use CT measurements of the enhancement curve to derive perfusion parameters (77).

Because contrast agents used for CT and MRI pass through the vascular endothelium but not cell membranes, effectively confining them to the plasma and the extracellular extravascular space, a two-compartment model can be used to derive quantitative parameters linked to physiologic characteristics (83,88). However, a two-compartment model is not applicable to the liver, which has both arterial and portal circulation. Additional enhancement curves must be measured in another tissue, such as the spleen; those data are then used to deconvolve separate values for the arterial and portal systems to determine the pharmacokinetic parameters (89). Tumor angiogenesis in the liver usually develops from the arterial blood supply and not from the portal circulation; thus, hepatic tumor circulation differs from the overall circulation pattern of this organ (10).

Several quantitative hemodynamic parameters have been established as standards (83): K^{trans} (min^{-1}), the rate of flux of contrast agent into the extracellular extravascular space within a given volume, or volume transfer constant (90); v_e , the volume of the extracellular extravascular space; and k_{ep} (min^{-1}), the rate constant for the back flux from the extracellular extravascular space to the vasculature. These parameters are related to each other by the equation, $k_{\text{ep}} = K^{\text{trans}}/v_e$. Several other names have been used for these same parameters, with some variations in the calculation methods (55,58). Wherever possible, we use the established terms k_{ep} , K^{trans} , and v_e in this review.

K^{trans} has several physiologic interpretations, depending on the balance between capillary permeability and blood flow. In situations in which capillary permeability is very high, the flux of the contrast agent into the extravascular extracellular space is limited by the flow rate. In this case, the kinetics follows the Kety model (59), and K^{trans} is equal to the blood plasma flow per unit volume of tissue.

When tracer flux is very low and blood flow is high, the blood plasma can be considered as a single pool, in which the concentration of contrast agent does not change substantially during the scan. Any change in signal is, therefore, due to the increase in the concentration of the contrast agent in the extravascular extracellular space. In this case, K^{trans} is equal to the product of the permeability and the surface area of the capillary vascular endothelium (i.e., K^{trans} is equal to the permeability surface area).

If the passage of contrast agent across the vasculature endothelium is limited by blood flow as well as by permeability, then the fractional reduction of capillary blood concentration of the contrast agent as it passes through the tissue must be taken into account. The rate of contrast agent flow out of the capillaries is initially high but decreases over time as the backflow of the contrast agent increases. The rate of clearance of the contrast agent from the system must also be accounted for by using a proportionality constant that links the concentration of the contrast agent to the rate of elimination of the agent from a compartment.

All of these situations fit into a generalized kinetic model, which can be expressed by the equation:

$$dC_t/dt = K^{\text{trans}}(C_p - C_t/v_e) = K^{\text{trans}}C_p - \kappa_{\text{ep}}C_t,$$

where C_t is the tracer concentration in tissue, C_p is the tracer concentration in plasma, and t is time (in seconds) (79). For CT, General Electric (Milwaukee, WI) provides a software package that uses kinetic modeling to map blood volume, flow, and K^{trans} (77).

In tumors, the accuracy of estimated blood flow from dynamic contrast imaging of angiogenic vasculature) may be limited because the flow in irregular-caliber vessels with nondichotomous branching is nonlaminar and because high vascular permeability leads to high viscosity due to hemoconcentration (87). Furthermore, neither the empirical semiquantitative parameters nor the quantitative parameters derived from pharmacokinetic modeling can be validated with an objective standard because they reflect a combination of morphology, hemodynamics, and vascular permeability.

Because differences in the value of K^{trans} may reflect changes in vascular permeability, capillary surface area, or a combination of the two, interpretation of the physiologic meaning of such changes is difficult. Experimental MRI contrast agents that have lower permeability, such as albumin-Gd-DTPA, or the very high-molecular-weight agents that remain confined within normal vasculature but not angiogenic vasculature, such as USPIO, may be more useful than the commonly used contrast agents for monitoring changes in permeability (131).

A few studies have addressed the reproducibility of some hemodynamic parameters (Table 4). Among the semiquantitative parameters, the maximum enhancement and the AUC appear to be the most reproducible. The slope or rate of enhancement appears to be the least reproducible, which may reflect the dependence of these measurements on the rate of injection of the contrast agent bolus as well as variations in cardiac input. Among the quantitative parameters, it appears that v_e has the least variability, with variation among patients being much greater than that within-patients. K^{trans} and k_{ep} also have sufficient reproducibility to be useful for measuring changes over time (Table 4).

IMAGING MOLECULAR MARKERS OF ANGIOGENESIS

Another approach to imaging angiogenic vasculature has been to develop molecular imaging agents that interact with

Table 4. Reproducibility of quantitative and semiquantitative kinetic hemodynamic parameters measured by magnetic resonance imaging with Gd-DPTA*

Parameter	Reproducibility	Variation (reference)
<i>Semiquantitative</i>		
AUC	Carcinomas and sarcomas (pretreatment repeat within 1 wk) Muscle (pretreatment repeat within 1 wk)	CoV = 12% (86)† CoV = 17% (86)
Maximum enhancement	Carcinomas and sarcomas (pretreatment repeat within 1 wk) Muscle (pretreatment repeat within 1 wk) Imaging before and after hormonal treatment for prostate cancer: Normal muscle Normal bone (ischium)	CoV = 9% (86)† CoV = 12% (86) CoV (range) = 19.5–29.3% (87) CoV = 23.1% (87)
Rate of enhancement	Glioma (repeat within 36–56 h) Carcinomas and sarcomas (pretreatment repeat within 1 wk) Muscle (pretreatment repeat within 1 wk)	CoV = 17.9% (max. rate); CoV = 7.1% (T_{90}) (58) CoV = 24%† (86) CoV = 28% (86)
<i>Quantitative</i>		
K^{trans} (volume transfer constant, min^{-1})	Glioma (repeat within 36–56 h) Carcinomas and sarcomas (pretreatment repeat within 1 wk) Glioma and astrocytoma (study repeat: within 2 days):	CoV = 7.7% (58) CoV = 24% (86)† CoV (range) = 0.02 – 6.34%; $r_1 = .997$ (55)
v_e (extravascular extracellular space)	Glioma (repeat within 36–56 h) Carcinomas and sarcomas (pretreatment repeat within 1 wk):Muscle (pretreatment repeat within 1 wk) Imaging before and after hormonal treatment for prostate cancer: Normal muscle Normal bone (ischium)	CoV = 6.2% (58) CoV = 8.5% (86) CoV = 16% (86) CoV (range) = 19.4 – 26.4% (87) CoV = 26.4% (87)
k_{ep} (rate constant, v_e to plasma, min^{-1})	Carcinomas and sarcomas (pretreatment repeat within 1 wk) Muscle (pretreatment repeat within 1 wk)	CoV = 21% (86) CoV = 49% (86)

*In some cases, names of imaging parameters used in the original article have been changed to those recommended by Tofts et al. (83). AUC = area under the enhancement curve from dynamic contrast imaging (in arbitrary units); K^{trans} = the rate of flux of contrast agent into the extracellular extravascular space within a given volume or volume transfer constant (in min^{-1}); v_e = the volume of the extracellular extravascular space; k_{ep} = the rate constant for the back flux from the extracellular extravascular space to the vasculature (in min^{-1}); CoV = coefficient of variance; T_{90} = time (in seconds) to reach 90% maximum enhancement.

†CoV of median values from individual voxel analysis, which was marginally better than CoV of mean values from analysis after whole tumor averaging.

characteristic molecular markers of angiogenic vasculature (7). Many molecular markers of angiogenesis have been identified (13,91), including vascular endothelial growth factor receptor (VEGFR-2), $\alpha_v\beta_3$ integrin, endoglin, and endosialin.

Because vascular endothelial cells are present in much smaller numbers than tumor cells, the density of angiogenic markers is low. Molecular agents for imaging angiogenesis must therefore bind to the markers with high specificity and be detectable at low concentrations. Thus, there is considerable interest in developing molecular imaging agents that can be detected by the most sensitive imaging modalities, PET, SPECT, and, to a lesser extent, ultrasound (with microbubble contrast agents) and optical imaging (with fluorescent contrast agents). In addition, even though the sensitivity of MRI is low, molecular imaging of angiogenesis is possible with oligomerized paramagnetic substances linked to an agent, such as an antibody, that binds a molecular marker of angiogenesis (92,93).

Many of the molecular imaging agents that have been developed to date have been used only to demonstrate the feasibility of their use in preclinical applications, and there are few data to assess the validity and reliability of this approach (Table 5). However, the potential of molecular imaging agents has been demonstrated in a phase I clinical trial that determined the pharmacokinetics of a monoclonal antibody targeted to VEGF, which was labeled with trace quantities of ^{124}I and imaged by PET (102).

CORRELATIONS BETWEEN IMAGING DATA AND HISTOPATHOLOGIC FINDINGS

Several studies have compared hemodynamic data derived from angiogenic imaging with microvessel density, which is a good prognostic indicator for many types of cancer, including malignant melanoma and breast, prostate, non-small-cell lung, cervical, bladder, esophageal, and gastrointestinal cancers (6). These studies have produced mixed results, with some but not all finding statistically significant correlations between data from imaging and microvascular density (Table 6). These discrepancies may possibly be explained by considering the differences in what is being measured. For example, the microvessel density of a biopsy sample is assessed histologically by counting the number of small blood vessels in a microscopic field that is similar in size to a single pixel of a CT or MR image and does not reflect the variation in blood volume seen in a tumor. Moreover, the number of vessels does not take into account capillary size, which is abnormal in angiogenic tumor vasculature and, therefore, likely to distort the relationship between vessel number and volume seen in normal tissues. Indeed, in a study of the angiogenic vasculature in an animal model of glioma, blood volume, determined by MRI, correlated well with the fractional volume, but not area, of blood vessels, determined microscopically in latex-filled microvessels (47) (Table 2). Furthermore, several studies have demonstrated that imaging data are more highly correlated with a pathology score, disease outcome, or the

Table 5. Imaging molecular markers of angiogenesis*

Molecular target	Contrast agent	Imaging modality	Comments	Application (reference)
AvB ₃ Integrin	¹⁸ F-RGD-containing glycopeptide	PET	Tumor enhancement 5.7 × background value	Melanoma xenograft (mouse) (94)
	¹²³ I-RGD-containing glycopeptide	SPECT	Minimal background uptake in tumor bearing limb; substantial uptake in intestine and thyroid	Mouse osteosarcoma (95)
	^{99m} Tc-RGD-containing peptide	SPECT	6/8 lymph node metastases and 11/11 other metastases detected	Human melanoma (96)
	¹¹¹ In-RP748 (Radiolabeled quinolone)	SPECT	Enhancement nearly 2 × control value	Canine myocardium (97)
	Echistatin-labeled microbubbles	Ultrasound	Acoustic intensity 1.7 × control value 14 days after implantation; 3.2 × control value after 28 days; linearly related to increase in tumor blood volume	Glioma xenograft (rat) (98)
	Antibody conjugated to liposome nanoparticles (65 nm) sequestering Gd-DTPA	MRI	Enhancement 1.6 × control value	Rabbit tumors (99); rabbit atherosclerosis (100)
VEGF receptor	¹²³ I-VEGF	SPECT	Overall tumor detection rate, 58% (n = 40)	Human gastrointestinal (101)
VEGF	¹²⁴ I-Ab	PET	Phase I clinical trial of Mab therapy	Human progressive solid tumors (102)
Endoglin (CD105, TGFβ receptor)	¹¹¹ I-Mab	Scintigraphy	Detected secondary tumor not seen with MRI	Human renal tumor, ex vivo (103)
ED-B fibronectin	¹²³ I-L19 (scFv) ₂ Ab fragment	SPECT	Overall detection rate, 84% (n = 19)	Human solid tumors (104)
Matrix metalloproteinase II	Quenched near infrared fluorochrome	Optical	Enhancement 8.5 × control value	Fibrosarcoma xenograft (mouse) (39)

*RGD = tripeptide containing Arg-Gly-Asp; Gd-DTPA = Gd-diethyltriamine pentaacetic acid; Mab = monoclonal antibody; Ab = antibody; PET = positron emission tomography; MRI = magnetic resonance imaging; SPECT = single-photon emission computed tomography; VEGF = vascular endothelial growth factor; TGFβ = tumor necrosis factor-β; ED-B = extradomain B fibronectin (exclusively produced in angiogenic vasculature).

overexpression of an angiogenesis promoter, VEGF, than with microvessel density (Table 6).

There is also evidence that angiogenic imaging data can be a useful predictor of response to chemoradiotherapy, the success of which depends on good perfusion of the tumor. In one study, microvessel density and VEGF expression did not correlate with survival in cervical cancer patients, whereas MRI estimates of k_{ep} and enhancement were statistically significant predictors of response to chemoradiotherapy and survival (105). In colorectal cancer, high values for K^{trans} (106) and low values for a perfusion index (a measurement that combines permeability and the rate of enhancement) (107) from MRI images were predictive of subsequent response to chemoradiotherapy. In head and neck cancers, CT estimates of blood flow predicted response to radiotherapy (108).

USING IMAGING TO MONITOR THERAPY

To date, it appears that, despite problems with instrument variability, dynamic contrast MRI has been used for most clinical studies of novel (119–124) and conventional therapies (125,126). PET, the most accurate and reliable modality, has been employed in a few clinical studies (102,127,128), CT has been used in other clinical studies (129), and intermittent sonography using a microbubble contrast agent has been used in preclinical studies (130).

There is no general agreement on which of the many imaging-derived hemodynamic parameters is the best for monitoring the response to therapy. MRI- or CT-determined quantitative parameters that are based on pharmacokinetic models, such as K^{trans} , k_{ep} ,

and v_e , are much less dependent on instrument and imaging protocol variation (83,88) than semiquantitative measures, such as the slope of enhancement or maximum change in image intensity. Therefore, it has been argued that parameters such as K^{trans} , k_{ep} , and v_e are more suitable for multicenter studies (58,88). Unfortunately, measurements of quantitative parameters with today's MRI instruments are much more sensitive to physiologic and machine noise than the empirical semiquantitative parameters. Both analytic approaches have their proponents and, fortunately, both acquire the dynamic data in roughly the same manner.

Because of the many potential sources of error in imaging, especially for MRI, as well as errors from modeling assumptions, reproducibility estimates obtained at one imaging center should not be used at another, especially if different equipment and protocols have been used. Galbraith et al. (86) have recommended that, in clinical trials of cancer therapy, two pretreatment scans of some patients should be performed to assess reproducibility of hemodynamic measurements at each center before treatment commences and that each pair of scans be read by a single reader who is not blinded to the positioning of the region of interest in first scan to improve reproducibility (86).

It is also important to use a parameter that is sensitive to wide variations in tumor physiology and is independent of within-patient variability that may be due, for example, to cardiac output and blood pressure. Another consideration for selection of a parameter is its sensitivity to the features of the microvasculature that are expected to change in response to therapy (86). Among the quantitative parameters, v_e exhibits the least within-patient variability due to physiologic changes but is sensitive to wide

Table 6. Correlation between imaging parameters and microvessel density (MVD) or pathologic condition*

Tumor type	Imaging modality (Contrast agent)	Parameter estimated	Pathologic condition or outcome	Correlation analysis	
				Imaging versus pathologic or disease outcome	Imaging versus MVD
Breast	MRI (USPIO)	fPV	SBR score	NS† <i>r</i> = .48, <i>P</i> > .01† <i>r</i> = .52, <i>P</i> > .05†§ <i>r</i> = .65, <i>P</i> > .01†§	NS (45)†‡
		K^{trans}		<i>r</i> = .70, <i>P</i> < .01† <i>r</i> = .67, <i>P</i> < .01‡ <i>r</i> = .80, <i>P</i> > .01†§ <i>r</i> = .94, <i>P</i> > .01‡§	NS†‡ (45)
	MRI (Gd-DTPA)	K^{trans}	Cancer versus benign	<i>P</i> < .001	<i>r</i> = .36, <i>P</i> < .01§ (109)
		Rate Amplitude k_{ep} Amplitude k_{ep}	VEGF expression	<i>P</i> < .05 NS <i>P</i> < .001 NS <i>P</i> < .005	<i>r</i> = .83, <i>P</i> < .001 (110) <i>P</i> < .05 (111) NS (111) NS (111) <i>P</i> < .005 <i>r</i> = .71, <i>P</i> < .07† (111)
Breast xenograft	MRI (albumin-Gd-DTPA)	K^{trans}	SBR score	<i>r</i> = .55, <i>P</i> < .0005†	<i>r</i> = .34, <i>P</i> < .05† (112)
		fPV	SBR score	<i>r</i> = .88, <i>P</i> < .001‡ <i>r</i> = .34, <i>P</i> < .05† NS‡	<i>r</i> = .67, <i>P</i> < .01‡ (51) NS (112)† NS (51)‡
	MRI (USPIO)	K^{trans} fPV	SBR score SBR score	<i>r</i> = .82, <i>P</i> < .001‡ NS‡	<i>r</i> = .76, <i>P</i> < .001 (51)‡ NS (51)‡
Cervical	MRI (Gd-DTPA)	k_{ep} Enhancement Amplitude Rate	VEGF expression	NS‡ NS‡ NS ‡ NS‡	NS‡ <i>P</i> < .05‡ <i>P</i> < .01‡ NS (113)
			Patient survival	<i>P</i> < .05‡ <i>P</i> < .0001‡ <i>P</i> < .001‡	<i>P</i> < .05‡ <i>P</i> < .01‡ NS (113)
Lung	CT (iodinated)	Attenuation	VEGF expression	<i>P</i> < .0001†	NS† <i>r</i> = .650, <i>P</i> < .001 (114)†‡
Oral	CT (iodinated)	Attenuation	Cancer versus benign	<i>P</i> < .005‡	<i>r</i> = .92, <i>P</i> < .000 (115)‡
Pancreas	CT (iodinated)	Attenuation	Tumor grade	<i>r</i> = .79, <i>P</i> < .001†	<i>r</i> = .68, <i>P</i> < .001 (116)†
Prostate	MRI (Gd-DTPA)	k_{ep}	Cancer versus PZ	<i>P</i> = .008†	<i>r</i> = .62, <i>P</i> < .001†
		Amplitude Rate	Gleason score	NS <i>P</i> = .025†	NS (117) NS (117)
Renal	CT (iodinated)	Attenuation	Clear cell versus other	<i>P</i> < .01†	<i>r</i> = .87, <i>P</i> < .01† (118)

*In some cases, names of imaging parameters used in original papers have been changed to those recommended by Tofts et al. (83). MRI = magnetic resonance imaging; USPIO = dextran-coated ultra-small particles of iron oxide; fPV = fractional plasma volume; SBR = Scarff-Bloom-Richardson; Gd-DTPA = gadolinium-diethyltriamine pentaacetic acid; K^{trans} = the rate of flux of contrast agent into the extracellular extravascular space within a given volume or volume transfer constant (in min^{-1}); amplitude = pharmacokinetic parameter of the tissue blood and interstitial volume, proportional to the degree of enhancement; rate = rate of enhancement; k_{ep} = the rate constant for the back flux from the extracellular extravascular space to the vasculature (in min^{-1}); VEGF = vascular endothelial growth factor; CT = computed tomography; PZ = normal peripheral zone tissue; NS = not significant; *r* = Pearson correlation coefficient.

†Whole tumor analysis.

‡“Hot spot” analysis.

§For malignant tumors only.

||For VEGF-negative tumors only.

variations within a population (86). On the other hand, K^{trans} is sensitive to vascular permeability, which may decrease in response to treatment (58,86).

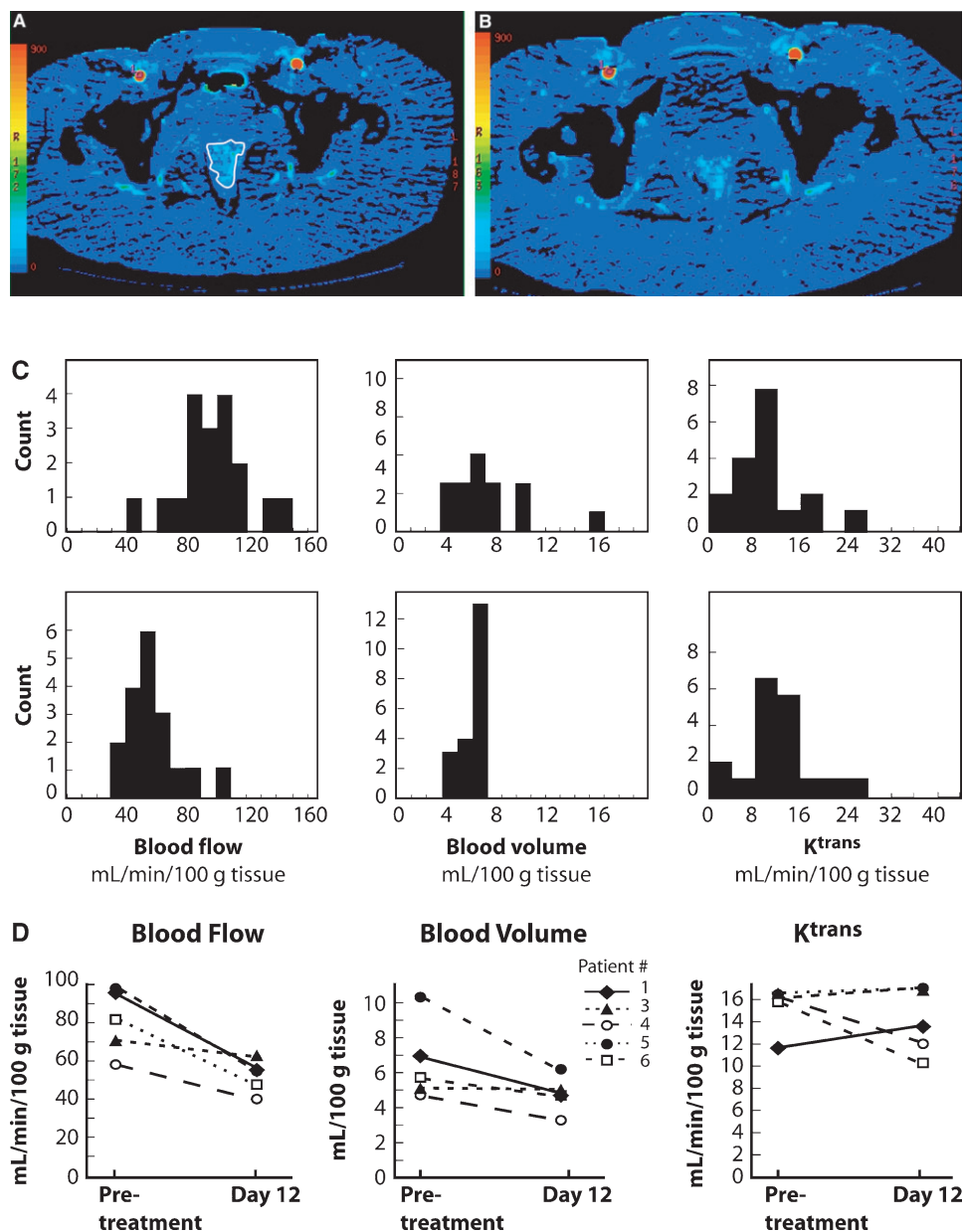
Data Analysis

There are several variations in the way imaging data can be quantified and presented. The raw data for analysis are obtained from the individual voxels of the image but, in some cases, the data from the whole tumor or from a hot spot has been averaged before analysis, whereas in other cases each voxel has been analyzed separately and presented as color maps, histograms, or

averaged data. Whole tumor averaging is the least sensitive to variables that are likely to change in repeated imaging, such as patient positioning or changes in tumor size, and data from observer-selected hot spots suffer from subjectivity and are the least reproducible (132). However, vascular changes in response to therapy observed in observer-selected or mathematically selected angiogenic hot spots are typically more statistically significant and are two to four times the magnitude of vascular changes measured by the whole tumor averaging (45,84) (Table 6).

Analyzing the data from each individual voxel separately combines the advantages of whole tumor and hot spot analysis methods and retains information about vascular heterogeneity

Fig. 2. Computerized tomography imaging data from a 56-year-old female who had rectal cancer and was treated with bevacizumab (Avastin, Genentech). **A** and **B**) Color maps of voxel-by-voxel analysis of blood flow, overlaying an anatomic image of pelvic region. The **small 1** and **circle** show the pixels used to derive the arterial input function for the calculations of hemodynamic parameters. The area outlined in **white** is the tumor. The color-coded scales on the **left** indicate tumor blood flow in milliliters per 100 g tissue per minute. **A**) Mean tumor blood flow (\pm standard deviation) before treatment (70 ± 15 mL/100 g/min). **B**) Twelve days after the patient received a single dose of drug (40 ± 16 mL/100 g/min). Images courtesy of Sanjeeva Kalva, MD, Massachusetts General Hospital. **C**) Histograms showing distributions of values for tumor blood flow (**left panels**), blood volume (**b**), and K^{trans} (the permeability surface area; **right panels**) from the same patient before (**top row**) and after (**bottom row**), showing a decrease in the number of tumor voxels with high blood flow and blood volume in the same region of interest after treatment. The tumor was randomly divided into multiple regions and each was analyzed separately. The vertical axis, count, refers to the number of regions that fell within a given range of blood flow, blood volume, and K^{trans} . **D**) Graphic representation of changes in mean blood flow, blood volume, and K^{trans} in each of six patients. From data of Willett et al. (129).



within the tumor but is much more demanding computationally than whole tumor averaging or hot spot analysis (86,87). Images that use color coding to show the range of values of the image derived vascular parameter can be aligned with anatomic images, and temporal changes in parameters can be easily visualized with the use of histograms that show the distribution of parameter values measured throughout the tumor (Fig. 2). Changes in parameter distribution can be calculated by comparing the frequency of values within a selected percentile or by statistical analysis using Spearman's rank-order correlation (133). Such distribution analysis is very sensitive to tumor progression and response to therapy (84,119,125). For example, in one small study of breast cancer, the distribution of K^{trans} corresponded to both morphologic and pathologic response to chemotherapy, whereas analysis of mean K^{trans} yielded a false-positive result (125).

In any study of the effectiveness of a therapy, it must be established that the change in the vasculature is tumor specific and not due to fluctuations in cardiac output, blood pressure, or

peripheral vascular resistance. These variables can be accounted for by determining vascular parameters of other healthy tissues and using those data to correct for global effects. Fat and bone are not enhanced sufficiently to be useful for this purpose, but muscle is. Even though blood volume and flow may vary with muscular tension, there are typically no consistent changes in these parameters over time (85,87). However, it may be necessary to consider specific factors that alter hemodynamics in muscle, such as insulin concentration (46). Finally, it must be established that the measured changes ultimately correspond to patient survival.

Monitoring Therapy in Clinical Trials

For imaging-derived parameters to fill the role of surrogate markers of drug response, vascular changes must be measurable within a short time after the start of treatment, dose dependent, and predictive of later clinical response.

Changes in vascular parameters can be rapid. For example, in a phase I clinical trial of the antineovascular agent, combretastatin A4 phosphate (OXIGENE, Watertown, MA), $^{15}\text{O}\text{-H}_2\text{O}$ and $^{11}\text{C}\text{O}$ PET detected statistically significant, tumor-specific decreases in tissue perfusion and blood volume within 30 minutes after administration of a single dose (128). MRI detected decreases in K^{trans} , v_e , and the AUC within 4 hours after the first dose of this drug (122). In other studies, the first posttreatment magnetic resonance images were acquired later after the start of treatment. For example, changes in the AUC were observed 24 hours after the initiation of the antivascular therapy, ZD6126 (*N*-acetylcholcholinol-*O*-phosphate; AstraZeneca, Macclesfield, U.K.), and were associated with later tumor necrosis in a preclinical study (119). In addition, changes in K^{trans} were observed 48 hours after the start of treatment with the anti-VEGF antibody HuMV833 in a clinical trial of progressive solid tumors (102). Similarly, changes in k_{ep} were observed in response to a VEGF tyrosine kinase inhibitor, PTK787/ZK22584, in both a preclinical study and a clinical trial for advanced colorectal cancer (123,134).

In most of these studies, the observed vascular response was dependent on the administered dose or on the plasma concentration of the active agent. The exception was the study of the HuMV833 antibody, which was found to have markedly variable distribution and clearance rates both within and between patients, as measured by PET imaging of additional trace quantities of ^{124}I -labeled antibody (102). However, distribution of the antibody was qualitatively associated with the distribution of k^{trans} as measured by MR dynamic contrast imaging. The wide variability in drug uptake by tumors suggests that pharmacokinetic imaging could be a useful method to ensure that an effective dose of drug is given to each patient. In addition, it illustrates the difficulty of comparing the biologic response of patients with various tumor histologic findings because they may have different dose requirements. Instead, the authors suggested treating a cohort of patients with an inpatient dose escalation in clinical trials and determining changes in pharmacokinetic parameters in individual tumors (102).

Finally, changes in vascular parameters must predict clinical response to be used as biomarkers. For example, glucocorticoids, which relieve symptoms in glioma patients but have no effect on patient outcome, reduce both blood volume and the diffusion of MRI contrast agents into tumors (135). Therefore, decreases in vascular parameters in response to a novel therapy cannot be presumed to predict clinical response. Nevertheless, decreases in vascular parameters appear, in some cases, to predict a clinical response. For example, in a recent clinical trial of the anti-VEGF antibody, bevacizumab (Avastin, Genentech, South San Francisco, CA) for treatment of rectal cancer, CT imaging showed a marked decrease in blood volume and flow 12 days after a single injection of the antibody in four of the five patients (Fig. 2). This early response was associated with subsequent tumor shrinkage observed after about 14 weeks of concurrent treatment with bevacizumab, conventional chemotherapy, and radiotherapy (129).

Other studies have demonstrated associations between the effects of conventional chemotherapeutic treatment on the vasculature and subsequent therapeutic response. In these studies, imaging was performed many weeks after initiation of treatment rather than a few days after treatment. Although the vascular changes were not measured early enough to be described as rapid, they were observed earlier than clinical measures of response. For example, MRI demonstrated that at 6–24 weeks after one cycle of chemotherapy for locally advanced breast

cancer, all patients who responded to therapy had a decrease in the number of voxels with an elevated value for K^{trans} , whereas nonresponders had an increase (84,125). In another study of locally advanced breast cancer, $^{15}\text{O}\text{-H}_2\text{O}$ PET showed that some patients had a marked decrease in blood flow after 2 months of chemotherapy, which correlated with subsequent clinical response, disease-free survival, and overall survival (127). Decreases in K^{trans} that correlate with subsequent tumor shrinkage have also been observed in response to androgen deprivation treatment for prostate cancer (126).

CONCLUDING REMARKS

The studies described above attest to the validity and reliability of several imaging techniques that have been used to determine vascular parameters. Measuring hemodynamic parameters related to blood volume, permeability, and blood flow through imaging has demonstrated potential for the rapid and noninvasive detection of vascular changes in tumors in response to therapy, which may predict later clinical response. If further studies confirm the predictive value of these changes, imaging may become a valuable biomarker in clinical studies for the determination of the appropriate clinical dose and for predicting the outcome of therapy. At this time, some of the imaging techniques require specialized facilities and/or software and are, therefore, not well suited to multicenter studies. Before the potential of imaging angiogenesis can be realized, it will be essential to standardize the imaging protocols as well as the analytic methods used within a study to enable accurate comparison of data and, especially for MRI, to establish the reproducibility of the measurements at each individual site.

REFERENCES

- (1) Folkman J. Role of angiogenesis in tumor growth and metastasis. *Semin Oncol* 2002;29:15–8.
- (2) Aiello L. Keeping in touch with angiogenesis. *Nat Med* 2000;6:379–81.
- (3) Rosen L. Antiangiogenic strategies and agents in clinical trials. *Oncologist* 2000;5 Suppl 1:20–7.
- (4) Marx J. A boost for tumor starvation. *Science* 2003;301:452–4.
- (5) Davis DW, McConkey DJ, Abbruzzese JL, Herbst RS. Surrogate markers in antiangiogenesis clinical trials. *Br J Cancer* 2003;89:8–14.
- (6) Hlatky L, Hahnfeldt P, Folkman J. Clinical application of antiangiogenic therapy: microvessel density, what it does and does not tell us. *J Natl Cancer Inst* 2002;94:883–93.
- (7) Costouros NG, Diehn FE, Libutti SK. Molecular imaging of tumor angiogenesis. *J Cell Biochem Suppl* 2002;39:72–8.
- (8) Anderson H, Price P, Blomley M, Leach MO, Workman P. Measuring changes in human tumour vasculature in response to therapy using functional imaging techniques. *Br J Cancer* 2001;85:1085–93.
- (9) Padhani A. Functional MRI for anticancer therapy assessment. *Eur J Cancer* 2002;38:2116–27.
- (10) Miles KA. Functional computed tomography in oncology. *Eur J Cancer* 2002;38:2079–84.
- (11) Jain RK, Munn LL, Fukumura D. Dissecting tumour pathophysiology using intravital microscopy. *Nat Rev Cancer* 2002;2:266–76.
- (12) Bergers G, Benjamin L. Tumorigenesis and the angiogenic switch. *Nat Rev Cancer* 2003;3:401–10.
- (13) McDonald D, Choyke P. Imaging of angiogenesis: from microscope to clinic. *Nat Med* 2003;9:713–25.
- (14) Miles K. Tumour angiogenesis and its relation to contrast enhancement on computed tomography. *Eur J Radiol* 1999;30:198–205.
- (15) van Dijke CF, Brasch RC, Roberts TP, Weidner N, Mathur A, Shames DM, et al. Mammary carcinoma model: correlation of macromolecular contrast-enhanced MR imaging characterizations of tumor microvasculature and histologic capillary density. *Radiology* 1996;198:813–8.

- (16) Anderson H, Price P. Clinical measurement of blood flow in tumours using positron emission tomography: a review. *Nucl Med Commun* 2002;23:131–8.
- (17) Lin PC. Optical imaging and tumor angiogenesis. *J Cell Biochem* 2003;90:484–91.
- (18) Dennie J, Mandeville JB, Boxerman JL, Packard SD, Rosen BR, Weisskoff RM. NMR imaging of changes in vascular morphology due to tumor angiogenesis. *Magn Reson Med* 1998;40:793–9.
- (19) Dunn JF, O'Hara JA, Zaim-Wadghiri Y, Lei H, Meyerand ME, Grinberg OY, et al. Changes in oxygenation of intracranial tumors with carbogen: A BOLD MRI and EPR oximetry study. *J Magn Reson Imaging* 2002;16:511–21.
- (20) Yetkin FZ, Mendelsohn D. Hypoxia imaging in brain tumors. *Neuroimaging Clin North Am* 2002;12:537–52.
- (21) Packard SD, Mandeville JB, Ichikawa T, Ikeda K, Terada K, Niloff S, et al. Functional response of tumor vasculature to PaCO₂: determination of total and microvascular blood volume by MRI. *Neoplasia* 2003;5:330–8.
- (22) Dunn AK, Devor A, Bolay H, Andermann ML, Moskowitz MA, Dale AM, et al. Simultaneous imaging of total cerebral hemoglobin concentration, oxygenation, and blood flow during functional activation. *Opt Lett* 2003;28:28–30.
- (23) Schirner M, Menrad A, Stephens A, Frenzel T, Hauff P, Licha K. Molecular imaging of tumor angiogenesis. *Ann N Y Acad Sci* 2004;1014:67–75.
- (24) Haubner R, Wester HJ. Radiolabeled tracers for imaging of tumor angiogenesis and evaluation of anti-angiogenic therapies. *Curr Pharm Des* 2004;10:1439–55.
- (25) Weissleder R, Bogdanov A Jr, Tung CH, Weinmann HJ. Size optimization of synthetic graft copolymers for in vivo angiogenesis imaging. *Bioconjug Chem* 2001;12:213–9.
- (26) Tournier H, Hyacinthe R, Schneider M. Gadolinium-containing mixed micelle formulations: a new class of blood pool MRI/MRA contrast agents. *Acad Radiol* 2002;9 Suppl 1:S20–8.
- (27) Storrs RW, Tropper FD, Li HY, Song CK, Sipkins DA, Kuniyoshi JK, et al. Paramagnetic polymerized liposomes as new recirculating MR contrast agents. *J Magn Reson Imaging* 1995;5:719–24.
- (28) Kobayashi H, Brechbiel MW. Dendrimer-based macromolecular MRI contrast agents: characteristics and application. *Mol Imaging* 2003;2:1–10.
- (29) Enochs WS, Harsh G, Hochberg F, Weissleder R. Improved delineation of human brain tumors on MR images using a long-circulating, superparamagnetic iron oxide agent. *J Magn Reson Imaging* 1999;9:228–32.
- (30) Harisinghani MG, Barents J, Hahn PF, Deserno WM, Tabatabaei S, van de Kaa CH, et al. Noninvasive detection of clinically occult lymph-node metastases in prostate cancer. *N Engl J Med* 2003;348:2491–9.
- (31) Rohren EM, Turkington TG, Coleman RE. Clinical applications of PET in oncology. *Radiology* 2004;231:305–32.
- (32) Ferrara KW, Merritt CR, Burns PN, Foster FS, Mattrey RF, Wickline SA. Evaluation of tumor angiogenesis with US: imaging, Doppler, and contrast agents. *Acad Radiol* 2000;7:824–39.
- (33) Li A, Miller E, Kilmer M, Brukilacchio T, Chaves T, Stott J, et al. Tomographic optical breast imaging guided by three-dimensional mammography. *Appl Opt* 2003;42: 5181–91.
- (34) Ntziachristos V, Yodh AG, Schnall MD, Chance B. MRI-guided diffuse optical spectroscopy of malignant and benign breast lesions. *Neoplasia* 2002;4:347–54.
- (35) Groner W, Winkelmann JW, Harris AG, Ince C, Bouma GJ, Messmer K, et al. Orthogonal polarization spectral imaging: a new method for study of the microcirculation. *Nat Med* 1999;5:1209–12.
- (36) Pahernik S, Harris AG, Schmitt-Sody M, Krasnici S, Goetz AE, Dellian M, et al. Orthogonal polarisation spectral imaging as a new tool for the assessment of antivasculature tumour treatment in vivo: a validation study. *Br J Cancer* 2002;86:1622–7.
- (37) Ntziachristos V, Yodh A, Schnall M, Chance B. Concurrent MRI and diffuse optical tomography of breast after indocyanine green enhancement. *Proc Natl Acad Sci U S A* 2000;97:2767–72.
- (38) Cuccia DJ, Bevilacqua F, Durkin AJ, Merritt S, Tromberg BJ, Gulsen G, et al. In vivo quantification of optical contrast agent dynamics in rat tumors by use of diffuse optical spectroscopy with magnetic resonance imaging coregistration. *Appl Opt* 2003;42:2940–50.
- (39) Bremer C, Bredow S, Mahmood U, Weissleder R, Tung CH. Optical imaging of matrix metalloproteinase-2 activity in tumors: feasibility study in a mouse model. *Radiology* 2001;221:523–9.
- (40) Phelps ME, Huang SC, Hoffman EJ, Kuhl DE. Validation of tomographic measurement of cerebral blood volume with C-11-labeled carboxyhemoglobin. *J Nucl Med* 1979;20:328–34.
- (41) Martin WR, Powers WJ, Raichle ME. Cerebral blood volume measured with inhaled C¹⁵O and positron emission tomography. *J Cereb Blood Flow Metab* 1987;7:421–6.
- (42) Inoue Y, Momose T, Machida K, Honda N, Mamiya T, Takahashi T, et al. Quantitation of cerebral blood volume by ^{99m}Tc-DTPA-HSA SPECT. *Radiat Med* 1992;10:184–8.
- (43) Sabatini U, Celsis P, Viallard G, Rascol A, Marc-Vergnes JP. Quantitative assessment of cerebral blood volume by single-photon emission computed tomography. *Stroke* 1991;22:324–30.
- (44) Kiessling F, Krix M, Heilmann M, Vosseler S, Lichy M, Fink C, et al. Comparing dynamic parameters of tumor vascularization in nude mice revealed by magnetic resonance imaging and contrast-enhanced intermittent power Doppler sonography. *Invest Radiol* 2003;38:516–24.
- (45) Rydland J, BjOrnerud A, Haugen O, Torheim G, Torres C, Kvistad KA, et al. New intravascular contrast agent applied to dynamic contrast enhanced MR imaging of human breast cancer. *Acta Radiol* 2003;44:275–83.
- (46) Raitakari M, Knuuti MJ, Ruotsalainen U, Laine H, Makea P, Teras M, et al. Insulin increases blood volume in human skeletal muscle: studies using [¹⁵O]CO and positron emission tomography. *Am J Physiol* 1995;269:E1000–5.
- (47) Pathak AP, Schmainda KM, Ward BD, Linderman JR, Rebro KJ, Greene AS. MR-derived cerebral blood volume maps: issues regarding histological validation and assessment of tumor angiogenesis. *Magn Reson Med* 2001;46:735–47.
- (48) Henry ME, Kaufman MJ, Lange N, Schmidt ME, Purcell S, Cote J, et al. Test-retest reliability of DSC MRI CBV mapping in healthy volunteers. *Neuroreport* 2001;12:1567–9.
- (49) Bremer C, Mustafa M, Bogdanov A, Ntziachristos N, Petrovsky A, Weissleder R. Steady-state blood volume measurements in experimental tumors with different angiogenic burdens—a study in mice. *Radiology* 2003;226:214–20.
- (50) Weissleder R, Cheng HC, Marecos E, Kwong K, Bogdanov A Jr. Non-invasive in vivo mapping of tumour vascular and interstitial volume fractions. *Eur J Cancer* 1998;34:1448–54.
- (51) Turetschek K, Huber S, Floyd E, Helbich T, Roberts TP, Shames DM, et al. MR imaging characterization of microvessels in experimental breast tumors by using a particulate contrast agent with histopathologic correlation. *Radiology* 2001;218:562–9.
- (52) Cenic A, Nabavi DG, Craen RA, Gelb AW, Lee TY. Dynamic CT measurement of cerebral blood flow: a validation study. *AJNR Am J Neuroradiol* 1999;20:63–73.
- (53) Cenic A, Nabavi DG, Craen RA, Gelb AW, Lee TY. A CT method to measure hemodynamics in brain tumors: validation and application of cerebral blood flow maps. *AJNR Am J Neuroradiol* 2000;21:462–70.
- (54) Ostergaard L, Smith DF, Vestergaard-Poulsen P, Hansen SB, Gee AD, Gjedde A, et al. Absolute cerebral blood flow and blood volume measured by magnetic resonance imaging bolus tracking: comparison with positron emission tomography values. *J Cereb Blood Flow Metab* 1998;18:425–32.
- (55) Li KL, Zhu XP, Checkley DR, Tessier JLL, Hillier VF, Waterton JC, et al. Simultaneous mapping of blood volume and endothelial permeability surface area product in gliomas using iterative analysis of first-pass dynamic contrast enhanced MRI data. *Br J Radiol* 2003;76:39–51.
- (56) Perko J, Aronen HJ, Kangasmaki A, Liu Y, Karonen J, Savolainen S, et al. Evaluation of four postprocessing methods for determination of cerebral blood volume and mean transit time by dynamic susceptibility contrast imaging. *Magn Reson Med* 2002;47:973–81.
- (57) Wirestam R, Ryding E, Lindgren A, Geijer B, Holtas S, Stahlberg F. Absolute cerebral blood flow measured by dynamic susceptibility contrast MRI: a direct comparison with Xe-133 SPECT. *Magma* 2000;11:96–103.
- (58) Jackson A, Jayson GC, Li KL, Zhu XP, Checkley DR, Tessier JJ, et al. Reproducibility of quantitative dynamic contrast-enhanced MRI in newly presenting glioma. *Br J Radiol* 2003;76:153–62.
- (59) Kety S. Measurement of local blood flow by the exchange of an inert diffusible substance. *Methods Med Res* 1960;8:228–36.
- (60) Raichle ME, Martin WR, Herscovitch P, Mintun MA, Markham J. Brain blood flow measured with intravenous H₂¹⁵O. II. Implementation and validation. *J Nucl Med* 1983;24:790–8.

- (61) Alpert NM, Eriksson L, Chang JY, Bergstrom M, Litton JE, Correia JA, et al. Strategy for the measurement of regional cerebral blood flow using short-lived tracers and emission tomography. *J Cereb Blood Flow Metab* 1984;4:28–34.
- (62) Roberts DA, Detre JA, Bolinger L, Insko EK, Leigh JS Jr. Quantitative magnetic resonance imaging of human brain perfusion at 1.5 T using steady-state inversion of arterial water. *Proc Natl Acad Sci U S A* 1994; 91:33–7.
- (63) Roberts DA, Detre JA, Bolinger L, Insko EK, Lenkinski RE, Pentecost MJ, et al. Renal perfusion in humans: MR imaging with spin tagging of arterial water. *Radiology* 1995;196:281–6.
- (64) Roberts DA, Gefter WB, Hirsch JA, Rizi RR, Dougherty L, Lenkinski RE, et al. Pulmonary perfusion: respiratory-triggered three-dimensional MR imaging with arterial spin tagging—preliminary results in healthy volunteers. *Radiology* 1999;212:890–5.
- (65) Matthew E, Andreason P, Carson RE, Herscovitch P, Pettigrew K, Cohen R, et al. Reproducibility of resting cerebral blood flow measurements with H₂¹⁵O positron emission tomography in humans. *J Cereb Blood Flow Metab* 1993;13:748–54.
- (66) Carroll TJ, Teneggi V, Jobin M, Squassante L, Treyer V, Hany TF, et al. Absolute quantification of cerebral blood flow with magnetic resonance, reproducibility of the method, and comparison with H₂¹⁵O positron emission tomography. *J Cereb Blood Flow Metab* 2002;22:1149–56.
- (67) Araujo LI, Lammertsma AA, Rhodes CG, McFalls EO, Iida H, Rechavia E, et al. Noninvasive quantification of regional myocardial blood flow in coronary artery disease with oxygen-15-labeled carbon dioxide inhalation and positron emission tomography. *Circulation* 1991;83:875–85.
- (68) Wilson CB, Lammertsma AA, McKenzie CG, Sikora K, Jones T. Measurements of blood flow and exchanging water space in breast tumors using positron emission tomography: a rapid and noninvasive dynamic method. *Cancer Res* 1992;52:1592–7.
- (69) Arbab AS, Aoki S, Toyama K, Miyazawa N, Kumagai H, Umeda T, et al. Quantitative measurement of regional cerebral blood flow with flow-sensitive alternating inversion recovery imaging: comparison with [iodine 123]-iodoamphetamine single photon emission CT. *AJNR Am J Neuroradiol* 2002;23:381–8.
- (70) Warmuth C, Gunther M, Zimmer C. Quantification of blood flow in brain tumors: comparison of arterial spin labeling and dynamic susceptibility-weighted contrast-enhanced MR imaging. *Radiology* 2003;228: 523–32.
- (71) Yen YF, Field AS, Martin EM, Ari N, Burdette JH, Moody DM, et al. Test-retest reproducibility of quantitative CBF measurements using FAIR perfusion MRI and acetazolamide challenge. *Magn Reson Med* 2002;47:921–8.
- (72) Wirestam R, Ryding E, Lindgren A, Geijer B, Ostergaard L, Andersson L, et al. Regional cerebral blood flow distributions in normal volunteers: dynamic susceptibility contrast MRI compared with ^{99m}Tc-HMPAO SPECT. *J Comput Assist Tomogr* 2000;24:526–30.
- (73) Wei K, Jayaweera AR, Firoozan S, Linka A, Skyba DM, Kaul S. Quantification of myocardial blood flow with ultrasound-induced destruction of microbubbles administered as a constant venous infusion. *Circulation* 1998;97:473–83.
- (74) Gillard JH, Minhas PS, Hayball MP, Bearcroft PW, Antoun NM, Freer CE, et al. Assessment of quantitative computed tomographic cerebral perfusion imaging with H₂¹⁵O positron emission tomography. *Neur Res* 2000; 22:457–64.
- (75) Kudo K, Terae S, Katoh C, Oka M, Shiga T, Tamaki N, et al. Quantitative cerebral blood flow measurement with dynamic perfusion CT using the vascular-pixel elimination method: comparison with H₂¹⁵O positron emission tomography. *AJNR Am J Neuroradiol* 2003;24:419–26.
- (76) Gillard JH, Antoun NM, Burnet NG, Pickard JD. Reproducibility of quantitative CT perfusion imaging. *Br J Radiol* 2001;74:552–5.
- (77) Miles KA, Griffiths MR. Perfusion CT: a worthwhile enhancement? *Br J Radiol* 2003;76:220–31.
- (78) Carroll TJ, Rowley HA, Haughton VM. Automatic calculation of the arterial input function for cerebral perfusion imaging with MR imaging. *Radiology* 2003;227:593–600.
- (79) Rijpkema M, Kaanders JH, Joosten FB, van der Kogel AJ, Heerschap A. Method for quantitative mapping of dynamic MRI contrast agent uptake in human tumors. *J Magn Reson Imaging* 2001;14:457–63.
- (80) Sorensen A, Reimer P. Cerebral MR perfusion imaging: principles and current applications. New York (NY): Verlag; 2000.
- (81) Wei K, Le E, Bin JP, Coggins M, Thorpe J, Kaul S. Quantification of renal blood flow with contrast-enhanced ultrasound. *J Am Coll Cardiol* 2001;37:1135–40.
- (82) Krix M, Kiessling F, Farhan N, Schmidt K, Hoffend J, Delorme S. A multivessel model describing replenishment kinetics of ultrasound contrast agent for quantification of tissue perfusion. *Ultrasound Med Biol* 2003; 29:1421–30.
- (83) Tofts PS, Brix G, Buckley DL, Evelhoch JL, Henderson E, Knopp MV, et al. Estimating kinetic parameters from dynamic contrast-enhanced T₁-weighted MRI of a diffusible tracer: standardized quantities and symbols. *J Magn Reson Imaging* 1999;10:223–32.
- (84) Hayes C, Padhani AR, Leach MO. Assessing changes in tumour vascular function using dynamic contrast-enhanced magnetic resonance imaging. *NMR Biomed* 2002;15:154–63.
- (85) Galbraith SM, Rustin GJ, Lodge MA, Taylor NJ, Stirling JJ, Jameson M, et al. Effects of 5,6-dimethylxanthenone-4-acetic acid on human tumor microcirculation assessed by dynamic contrast-enhanced magnetic resonance imaging. *J Clin Oncol* 2002;20:3826–40.
- (86) Galbraith SM, Lodge MA, Taylor NJ, Rustin GJ, Bentzen S, Stirling JJ, et al. Reproducibility of dynamic contrast-enhanced MRI in human muscle and tumours: comparison of quantitative and semi-quantitative analysis. *NMR Biomed* 2002;15:132–42.
- (87) Padhani AR, Hayes C, Landau S, Leach MO. Reproducibility of quantitative dynamic MRI of normal human tissues. *NMR Biomed* 2002;15: 143–53.
- (88) Brix G, Bahner ML, Hoffmann U, Horvath A, Schreiber W. Regional blood flow, capillary permeability, and compartmental volumes: measurement with dynamic CT—initial experience. *Radiology* 1999;210: 269–76.
- (89) Fuentes MA, Keith CJ, Griffiths M, Durbridge G, Miles KA. Hepatic haemodynamics: interrelationships between contrast enhancement and perfusion on CT and Doppler perfusion indices. *Br J Radiol* 2002;75:17–23.
- (90) Patlak CS, Fenstermacher JD. Measurements of dog blood-brain transfer constants by ventriculocisternal perfusion. *Am J Physiol* 1975;229: 877–84.
- (91) Carmeliet P. Angiogenesis in health and disease. *Nat Med* 2003;9: 653–60.
- (92) Curtet C, Maton F, Havet T, Slinkin M, Mishra A, Chatal JF, et al. Polylysine-Gd-DTPAn and polylysine-Gd-DOTAn coupled to anti-CEA F(ab)² fragments as potential immunoccontrast agents. Relaxometry, biodistribution, and magnetic resonance imaging in nude mice grafted with human colorectal carcinoma. *Invest Radiol* 1998;33:752–61.
- (93) Bogdanov A Jr, Matuszewski L, Bremer C, Petrovsky A, Weissleder R. Oligomerization of paramagnetic substrates results in signal amplification and can be used for MR imaging of molecular targets. *Mol Imaging* 2002;1:16–23.
- (94) Haubner R, Wester HJ, Weber WA, Mang C, Ziegler SI, Goodman SL, et al. Noninvasive imaging of $\alpha_v\beta_3$ integrin expression using ¹⁸F-labeled RGD-containing glycopeptide and positron emission tomography. *Cancer Res* 2001;61:1781–5.
- (95) Haubner R, Wester HJ, Burkhart F, Senekowitsch-Schmidtke R, Weber W, Goodman SL, et al. Glycosylated RGD-containing peptides: tracer for tumor targeting and angiogenesis imaging with improved biokinetics. *J Nucl Med* 2001;42:326–36.
- (96) Sivolapenko GB, Skarlos D, Pectasides D, Stathopoulou E, Milonakis A, Sirmalis G, et al. Imaging of metastatic melanoma utilizing a technetium-99m labelled RGD-containing synthetic peptide. *Eur J Nucl Med* 1998;25:1383–9.
- (97) Meoli DF, Sadeghi MM, Krassilnikova S, Bourke BN, Giordano FJ, Dione DP, et al. Noninvasive imaging of myocardial angiogenesis following experimental myocardial infarction. *J Clin Invest* 2004;113:1684–91.
- (98) Ellegala D, Leong-Poi H, Carpenter J, Klibanov A, Kaul S, Shaffrey M, et al. Imaging tumor angiogenesis with contrast ultrasound and microbubbles targeted to $\alpha_v\beta_3$. *Circulation* 2003;108:336–41.
- (99) Winter PM, Caruthers SD, Kassner A, Harris TD, Chinen LK, Allen JS, et al. Molecular imaging of angiogenesis in nascent Vx-2 rabbit tumors using a novel $\alpha_v\beta_3$ -targeted nanoparticle and 1.5 tesla magnetic resonance imaging. *Cancer Res* 2003;63:5838–43.

- (100) Winter PM, Morawski AM, Caruthers SD, Fuhrhop RW, Zhang H, Williams TA, et al. Molecular imaging of angiogenesis in early-stage atherosclerosis with $\alpha_v\beta_3$ -integrin-targeted nanoparticles. *Circulation* 2003;108:2270–4.
- (101) Li S, Peck-Radosavljevic M, Kienast O, Preitfellner J, Hamilton G, Kurtaran A, et al. Imaging gastrointestinal tumours using vascular endothelial growth factor-165 (VEGF165) receptor scintigraphy. *Ann Oncol* 2003;14:1274–7.
- (102) Jayson GC, Zweit J, Jackson A, Mulatero C, Julyan P, Ranson M, et al. Molecular imaging and biological evaluation of HuMV833 anti-VEGF antibody: implications for trial design of antiangiogenic antibodies. *J Natl Cancer Inst* 2002;94:1484–93.
- (103) Duff SE, Li C, Garland JM, Kumar S. CD105 is important for angiogenesis: evidence and potential applications. *FASEB J* 2003;17:984–92.
- (104) Santimaria M, Moscatelli G, Viale GL, Giovannoni L, Neri G, Viti F, et al. Immunoscintigraphic detection of the ED-B domain of fibronectin, a marker of angiogenesis, in patients with cancer. *Clin Cancer Res* 2003;9:571–9.
- (105) Mayr NA, Hawighorst H, Yuh WT, Essig M, Magnotta VA, Knopp MV. MR microcirculation assessment in cervical cancer: correlations with histomorphological tumor markers and clinical outcome. *J Magn Reson Imaging* 1999;10:267–76.
- (106) George ML, Dzik-Jurasz AS, Padhani AR, Brown G, Tait DM, Eccles SA, et al. Non-invasive methods of assessing angiogenesis and their value in predicting response to treatment in colorectal cancer. *Br J Surg* 2001;88:1628–36.
- (107) de Vries A, Griebel J, Kremser C, Judmaier W, Gneiting T, Debbage P, et al. Monitoring of tumor microcirculation during fractionated radiation therapy in patients with rectal carcinoma: preliminary results and implications for therapy. *Radiology* 2000;217:385–91.
- (108) Hermans R, Meijerink M, Van den Bogaert W, Rijnders A, Weltens C, Lambin P. Tumor perfusion rate determined noninvasively by dynamic computed tomography predicts outcome in head-and-neck cancer after radiotherapy. *Int J Radiat Oncol Biol Phys* 2003;57:1351–6.
- (109) Hulka CA, Edmister WB, Smith BL, Tan L, Sgroi DC, Campbell T, et al. Dynamic echo-planar imaging of the breast: experience in diagnosing breast carcinoma and correlation with tumor angiogenesis. *Radiology* 1997;205:837–42.
- (110) Buadu LD, Murakami J, Murayama S, Hashiguchi N, Sakai S, Masuda K, et al. Breast lesions: correlation of contrast medium enhancement patterns on MR images with histopathologic findings and tumor angiogenesis. *Radiology* 1996;200:639–49.
- (111) Knopp MV, Weiss E, Sinn HP, Mattern J, Junkermann H, Radeleff J, et al. Pathophysiologic basis of contrast enhancement in breast tumors. *J Magn Reson Imaging* 1999;10:260–6.
- (112) Turetschek K, Floyd E, Shames DM, Roberts TP, Preda A, Novikov V, et al. Assessment of a rapid clearance blood pool MR contrast medium (P792) for assays of microvascular characteristics in experimental breast tumors with correlations to histopathology. *Magn Reson Med* 2001;45:880–6.
- (113) Hawighorst H, Knapstein PG, Knopp MV, Weikel W, Brix G, Zuna I, et al. Uterine cervical carcinoma: comparison of standard and pharmacokinetic analysis of time-intensity curves for assessment of tumor angiogenesis and patient survival. *Cancer Res* 1998;58:3598–602.
- (114) Tateishi U, Kusumoto M, Nishihara H, Nagashima K, Morikawa T, Moriyama N. Contrast-enhanced dynamic computed tomography for the evaluation of tumor angiogenesis in patients with lung carcinoma. *Cancer* 2002;95:835–42.
- (115) Hayashi K, Tozaki M, Sugisaki M, Yoshida N, Fukuda K, Tanabe H. Dynamic multislice helical CT of ameloblastoma and odontogenic keratocyst: correlation between contrast enhancement and angiogenesis. *J Comput Assist Tomogr* 2002;26:922–6.
- (116) Wang ZQ, Li JS, Lu GM, Zhang XH, Chen ZQ, Meng K. Correlation of CT enhancement, tumor angiogenesis and pathologic grading of pancreatic carcinoma. *World J Gastroenterol* 2003;9:2100–4.
- (117) Schlemmer HP, Merkle J, Grobholz R, Jaeger T, Michel MS, Werner A, et al. Can pre-operative contrast-enhanced dynamic MR imaging for prostate cancer predict microvessel density in prostatectomy specimens? *Eur Radiol* 2004;14:309–17.
- (118) Jinzaki M, Tanimoto A, Mukai M, Ikeda E, Kobayashi S, Yuasa Y, et al. Double-phase helical CT of small renal parenchymal neoplasms: correlation with pathologic findings and tumor angiogenesis. *J Comput Assist Tomogr* 2000;24:835–42.
- (119) Robinson S, McIntyre D, Checkley D, Tessier J, Howe F, Griffiths J, et al. Tumour dose response to the antivascular agent ZD6126 assessed by magnetic resonance imaging. *Br J Cancer* 2003;88:1592–7.
- (120) Stevenson JP, Rosen M, Sun W, Gallagher M, Haller DG, Vaughn D, et al. Phase I trial of the antivascular agent combretastatin A4 phosphate on a 5-day schedule to patients with cancer: magnetic resonance imaging evidence for altered tumor blood flow. *J Clin Oncol* 2003;21:4428–38.
- (121) Thomas JP, Arzoumanian RZ, Alberti D, Marnocha R, Lee F, Friedl A, et al. Phase I pharmacokinetic and pharmacodynamic study of recombinant human endostatin in patients with advanced solid tumors. *J Clin Oncol* 2003;21:223–31.
- (122) Galbraith SM, Maxwell RJ, Lodge MA, Tozer GM, Wilson J, Taylor NJ, et al. Combretastatin A4 phosphate has tumor antivascular activity in rat and man as demonstrated by dynamic magnetic resonance imaging. *J Clin Oncol* 2003;21:2831–42.
- (123) Morgan B, Thomas A, Dreves J, Hennig J, Buchert M, Jivan A, et al. Dynamic contrast-enhanced magnetic resonance imaging as a biomarker for the pharmacological response of PTK787/ZK 222584, an inhibitor of the vascular endothelial growth factor receptor tyrosine kinases, in patients with advanced colorectal cancer and liver metastases: results from two phase I studies. *J Clin Oncol* 2003;21:3955–64.
- (124) Bhujwala Z, Artemov D, Natarajan K, Solaiyappan M, Kollars P, Kristjansen P. Reduction of vascular and permeable regions in solid tumors detected by macromolecular contrast magnetic resonance imaging after treatment with antiangiogenic agent TNP-470. *Clin Cancer Res* 2003;9:355–62.
- (125) Delille J-P, Slanetz P, Yeh E, Halpern E, Kopans D, Garrido L. Invasive ductal breast carcinoma response to neoadjuvant chemotherapy: noninvasive monitoring with functional MR imaging—pilot study. *Radiology* 2003;228:63–9.
- (126) Padhani AR, MacVicar AD, Gapinski CJ, Dearnaley DP, Parker GJ, Suckling J, et al. Effects of androgen deprivation on prostatic morphology and vascular permeability evaluated with MR imaging. *Radiology* 2001;218:365–74.
- (127) Mankoff D, Dunnwald L, Gralow J, Ellis G, Schubert E, Tseng J, et al. Changes in blood flow and metabolism in locally advanced breast cancer treated with neoadjuvant chemotherapy. *J Nucl Med* 2003;44:1806–14.
- (128) Anderson HL, Yap JT, Miller MP, Robbins A, Jones T, Price PM. Assessment of pharmacodynamic vascular response in a phase I trial of combretastatin A4 phosphate. *J Clin Oncol* 2003;21:2823–30.
- (129) Willett CG, Boucher Y, Di Tomaso E, Duda DG, Munn LL, Tong RT, et al. Direct evidence that the VEGF-specific antibody bevacizumab has antivascular effects in human rectal cancer. *Nat Med* 2004;10:145–7. Epub 2004 Jan 25.
- (130) Krix M, Kiessling F, Vosseler S, Farhan N, Mueller MM, Bohlen P, et al. Sensitive noninvasive monitoring of tumor perfusion during antiangiogenic therapy by intermittent bolus-contrast power Doppler sonography. *Cancer Res* 2003;63:8264–70.
- (131) Roberts T, Turetschek K, Preda A, Novikov V, Moeglich M, Shames D, et al. Tumor microvascular changes to anti-angiogenic treatment assessed by MR contrast media of different molecular weights. *Acad Radiol* 2002;9 Suppl 2:S111–3.
- (132) Wetzel SG, Cha S, Johnson G, Lee P, Law M, Kasow DL, et al. Relative cerebral blood volume measurements in intracranial mass lesions: interobserver and intraobserver reproducibility study. *Radiology* 2002;224:797–803.
- (133) Dawson B, Trapp R. Basic and clinical biostatistics. 3rd ed. New York (NY): McGraw-Hill; 2001.
- (134) Thomas AL, Morgan B, Dreves J, Unger C, Wiedenmann B, Vanhoefer U, et al. Vascular endothelial growth factor receptor tyrosine kinase inhibitors: PTK787/ZK 222584. *Semin Oncol* 2003;30:32–8.
- (135) Ostergaard L, Hochberg FH, Rabinov JD, Sorensen AG, Lev M, Kim L, et al. Early changes measured by magnetic resonance imaging in cerebral blood flow, blood volume, and blood-brain barrier permeability following dexamethasone treatment in patients with brain tumors. *J Neurosurg* 1999;90:300–5.

NOTES

H. H. Pien holds stock in Pfizer and Amgen and has an equity position in SRU Biosystems (Woburn, MA). A. G. Sorensen has received research support from, has consulted for, or has spoken on behalf of the following companies: Siemens Medical Systems, General Electric Medical Systems, Glaxo SmithKline, Novartis Pharmaceuticals, Descartes Therapeutics, Schering AG,

Hemedex, Inc., Pfizer, Inc., StemCells, Inc., and Transkaryotic Therapies, Inc. In addition, Dr. Sorensen has an equity position in and holds the position of Medical Director at EPIX Medical, Inc. (Cambridge, MA), a specialty pharmaceutical company engaged in developing targeted contrast agents for cardiovascular MRI.

Manuscript received May 24, 2004; revised August 4, 2004; accepted November 30, 2004.